HIGH IMPEDANCE SURFACES BASED ANTENNAS FOR HIGH DATA RATE COMMUNICATIONS AT 40 GHz

C. M. Tran, H. Hafdallah Ouslimani, L. Zhou and A. C. Priou

Université Paris Ouest Nanterre La Défense
Laboratoire Energétique Mécanique Electromagnétisme, LEME
50 rue de Sèvres, Ville d'Avray 92410 Ville d'Avray, France

H. Teillet and J.-Y. Daden

Thales Communications
160 Boulevard de Valmy, Colombes 92704, France

A. Ourir

Institut Langevin, LOA
ESPCI, CNRS UMR 7587, 10 rue Vauquelin 75005 Paris, France

Abstract—Millimeter wave High Impedance Surfaces (HIS) based antennas are designed, fabricated, and characterized for high data rate communications at frequencies around 40 GHz. HIS with different finite surface area sizes are used as a ground plane for the microstrip patch antennas to suppress the surface waves. The antenna measurements and full wave electromagnetic simulations demonstrate a wide bandwidth of 12–15% in the frequency range of 38–44 GHz with a high gain of ∼ 6 dB and a very low cross polar contribution better than −20 dB.

1. INTRODUCTION

The millimeter-wave length high bit rate communications concern a large domain of the modern applications such as the radio frequency modules dedicated to the Hertzian infrastructures, wireless stations, automotive radar and 2/3/4G cellular mobile [1–5]. Recent researches in the field of metamaterials have led to the development of promising

---

Corresponding author: H. Hafdallah Ouslimani (habiba.ouslimani@u-paris10.fr).

new microwave and millimeter-wave devices which are crucial in designing high bit rate communication systems. Several industrial and academic research laboratories and world class clusters (such as the French "System@tic" cluster) have developed considerable programs to design new types of electromagnetic components and devices based on metamaterials.

It is known that the microstrip antennas radiate into the free space but also excite the undesirable surface wave (SW) modes [6, 7]. For substrates of finite size, the surface wave fields will diffract from the edges of the substrate and degrade the overall performances of the antennas [6, 7]. To prohibit the propagation of electromagnetic waves at certain frequencies, Sievenpiper et al. have developed the High Impedance Surfaces (HIS) which represent a type of electromagnetic band gap (EBG) material [8, 9]. HIS are usually composed of a periodic pattern of various metallization all connected to the ground plane by metal vias. The fundamental new electromagnetic properties of the HIS [8–10] are now intensively used in the antenna and filter applications [11–14]. These properties allow the HIS to operate as a magnetic wall in front of an incident wave because they have very high surface impedance within the HIS resonant band [8–10]. This allows the antenna to lie directly adjacent to the ground plane without being shorted out. This leads to low profile antenna designs where the radiating elements are restricted to limited spaces [15–18]. These properties also allow the HIS to have a forbidden frequency band over which neither surface waves nor currents can propagate [8–10, 16]. The HIS work as EM barriers used to partially isolate the radiating elements from their proper excited SWs which diffract from the edges of the substrate of finite size and from the nearby electromagnetic surroundings [2, 3, 13, 14]. This leads to reducing the near field behind the antenna, resulting in a general increase of the antenna efficiency without any bandwidth reduction [17, 18].

In this paper, we present mushroom-like HIS structures implemented into several microstrip antenna designs. The microstrip patch antenna is surrounded by a limited number of rows (N-Layer) of HIS unit cells. The HIS based antenna is designed for high data rate communications and operates at a frequency of 40 GHz. HIS based antenna prototypes with different sizes have been fabricated and characterized to study the effects of the HIS size on the antenna's performances. The return loss, bandwidth and radiation patterns of the HIS based antennas are compared to the conventional design in order to appreciate the benefits of HIS.

2. HIGH IMPEDANCE SURFACE DESIGN

2.1. HIS with Infinite Periodic Size

The high-impedance electromagnetic surface studied here is the mushroom-like structure shown in Figure 1(a). The unit cell is composed of a metallic patch connected to the ground plane with a metallic via. It is defined as in Sivenpiper's work [8, 9]. In EM simulator CST, the unit mushroom-like cell is simulated using boundary conditions on the four sides to ensure an infinite periodicity in the horizontal plane. The period of the HIS is 1054 μm. The gap width between the patches is 157 μm. The metal plated vias have a diameter of 200 μm. The patches are separated from the metallic ground plane layer by a 510 μm thick Duroïd substrate (Rogers 4003: $\varepsilon_r = 3.58$ and $\tan\delta = 0.002$). The calculated reflection coefficient of the infinite size HIS array under normal incidences is presented in Figure 1(b). The reflection phase varies continuously from $+180°$ to $-180°$ and crosses zero at the resonance frequency of 40 GHz. At this frequency, the reflector losses are ~ -0.12 dB, and the surface impedance is high. The bandwidth is of 42% and centred at 40 GHz. The resonant HIS surface can be modeled by an equivalent LC circuit [8, 9] where the fringing electric fields between adjacent patches produce capacitances, while the vias form inductances. The high-impedance properties occur near the resonance frequency given by $f_0 = 1/2\pi\sqrt{LC}$.
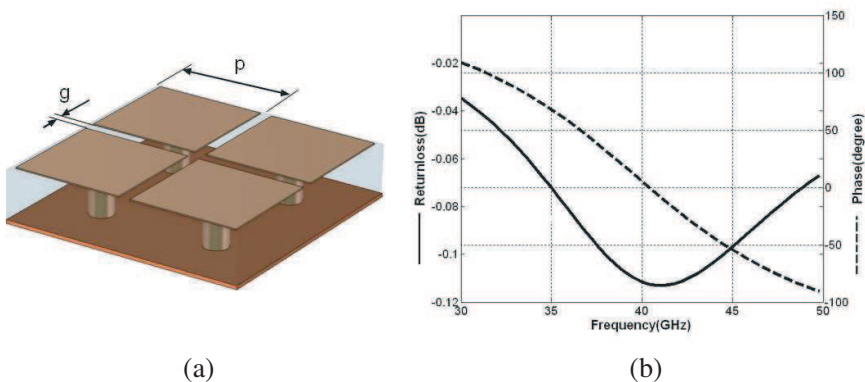

(a)   (b)

Figure 1. (a) investigated Mushroom-like HIS ($p = 1054\,\mu m$, $g = 157\,\mu m$), (b) magnitude and phase of the reflection coefficient under a normal incidence.
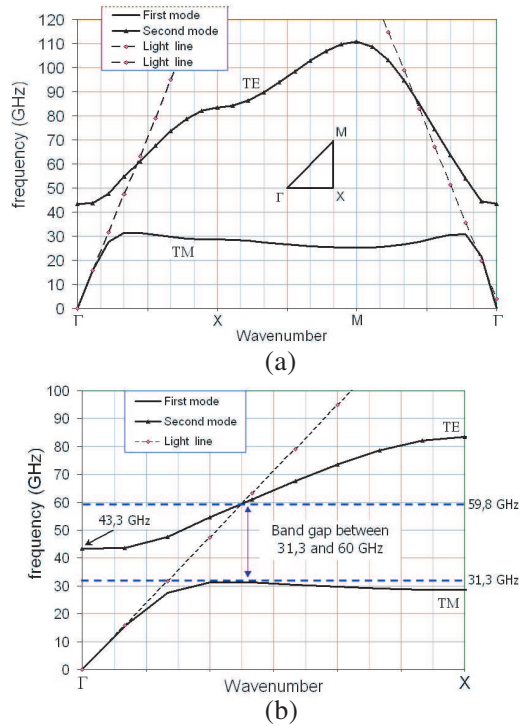
Figure 2. Dispersion diagram of the Mushroom-like HIS; (a) in the 2D directions (kx, ky) of the Brillouin zone and (b) zoom in the kx direction from Γ to X. The black dashed lines show the light lines. Under the light lines a SW band gap is observed between 31.3 GHz and 59.8 GHz. Above the light line and starting from $f = 43.3$ GHz leaky wave's mode can radiates in the free space.

Figure 2 depicts the dispersion diagram of the infinite mushroom-like HIS which allows us to deduce the characteristics of the propagating waves and the electromagnetic band gap. Bound surface waves occupy the region below the light lines. Below the resonance frequency, the HIS supports propagating TM surface waves. Above this frequency, it supports propagating TE surface waves. The surface wave band gap is observed between 31.3 GHz (TM mode edge) and 59.8 GHz (TE mode edge). Within this range, no EM polarization produces significant transmission. Above the light lines, in a limited frequency range starting from 43.3 GHz, TE modes leaky waves exist and can radiate efficiently into the free space. Figure 2(b) gives the same HIS dispersion diagram but limited to the first reduced Brillouin zone from Γ to X.
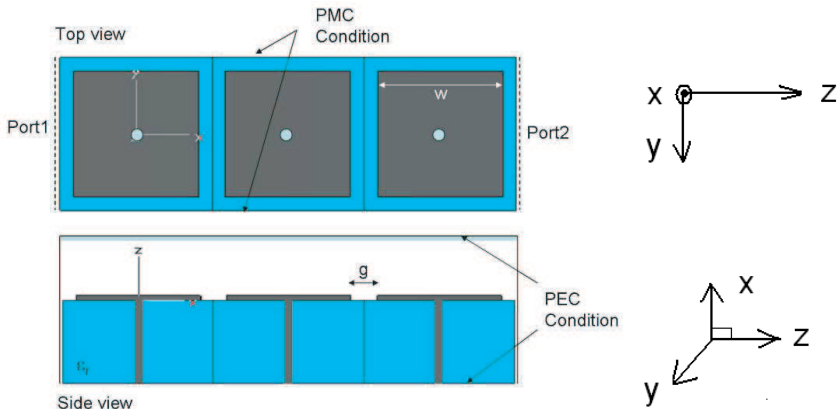
Figure 3. TEM wave guide setup, the N unit cells of the Mushroom-like HIS (Here $N = 3$) are disposed along the direction of propagation (oz). The TEM wave guide model is implemented in CST Microwave Studio.

2.2. HIS with Finite Size N-unit Periodic Cells

We have investigated the surface wave band gap of an HIS composed by a limited number of unit cells. The choice of a sufficient unit cell number (the smaller) is important to designing compact structure antennas. Figure 3 depicts the TEM waveguide setup [10, 11] utilized to determine the transmission and the reflection parameters of the finite size HIS array. The HIS is implemented inside the wave guide as seen in Figure 3. Herein, this number is varied from 1 to 6. In this configuration the HIS is supposed to be periodic and infinite in the oy direction and finite and composed by N unit cells in the oz direction of the propagation (Figure 3). The waveguide has perfect electric conductor (PEC) boundary conditions for the two parallel horizontal sides and perfect magnetic conductor (PMC) for the other two sides.

We have used the 3D EM simulator CST Microwave Studio to simulate the magnitude of transmission coefficients for N varying up to 6 (Figure 4). The strong modifications of the band gap shape both in width and depth demonstrate the influence of the HIS unit cell number. The band gap is enlarged with N and becomes stable for $N \geq 6$ [10, 11]. An attenuation of the transmission below -30 dB is obtained only for $N \geq 3$. Table 1 gives the band gap width obtained for $N = 3$ to 6 under the criteria S_{21} (dB) below -30 dB. For $N = 2$, the transmission curve is under -20 dB over a wide frequency range of 33–59 GHz. This result is coherent with the band gap width of the infinite size HIS determined from the dispersion curve (Figure 2).

Table 1. Band gap width for a finite size HIS array, f_{c1} and f_{c2} are the low and high cutoff frequencies, N is the number of unit cells in the direction of propagation.

S_{21} (dB) < -30 dB			
N	f_{c1} (GHz)	f_{c2} (GHz)	Band gap (GHz)
3	32	61	29
4	31	63	32
5	31	64	33
6	31	65	34

(a)   (b)
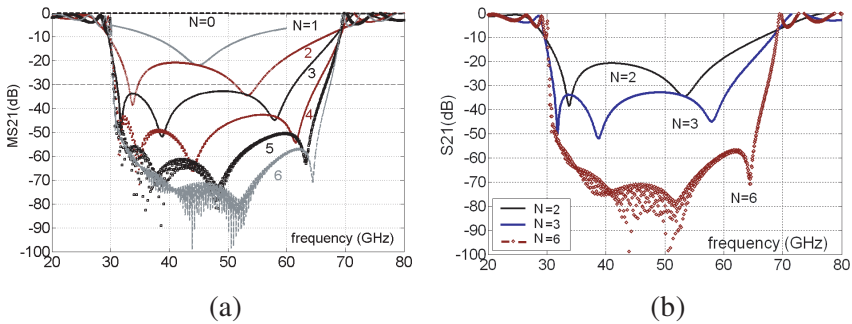
Figure 4. Magnitude of the transmission S_{21} parameter for various numbers of HIS unit cells, (a) $N = 1$, 2 to 6 and (b) $N = 2$, 3 and 6.

When we compare the different cases of Figure 4, particularly around the operational frequency of 40 GHz, the difference between the cases $N = 2$ and $N = 3$ is more important than that between $N = 1$ and $N = 2$ and that between $N = 3$ and $N = 4$. It appears very interesting to study the influence of limited number N on the overall antenna performances, particularly for the configurations $N = 2$ and $N = 3$. It is the reason that we realized and characterized two prototype antennas with finite size HIS array, $N = 2$ and $N = 3$.

3. ANTENNA DESIGN

Figure 5(a) depicts a rectangular microstrip patch antenna with 1.607 mm × 1.679 mm dimensions. It is designed to operate around 40 GHz inside the working HIS SW band gap. It is etched on the substrate dielectric layer Rogers 4003 ($\varepsilon_r = 3.58$ and $h = 0.51$ mm)
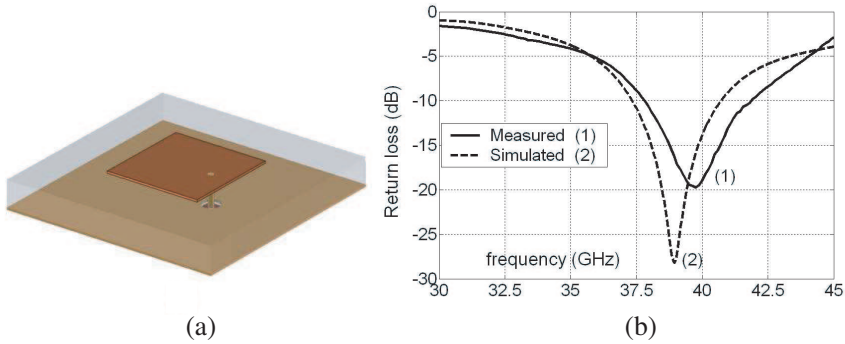
Figure 5. (a) Coax fed printed patch antenna, (b) measured and simulated return loss (S_{11}) of the designed patch antenna.

and fed using a coaxial probe. Figure 5(b) presents the measured and calculated return losses (S_{11}) of the conventional patch antenna. The simulation results show a resonance frequency of $\sim 38.5\,\text{GHz}$ and a band width under $-10\,\text{dB}$ in the frequency range of 37.5–41 GHz. The measurement shows a resonance frequency of 39.5 GHz and a bandwidth in the range of 38–42 GHz which is a rather good bandwidth for this frequency range (12%). The differences between the simulation and measurement are due to the substrate losses and manufacturing imperfections.

Figures 6(a) and 6(b) show the calculated and measured antenna radiation patterns in E and H planes at the resonance frequency of the antenna. The simulations of Figure 6(a) give a gain of $\sim 5\,\text{dB}$ in both E- and H-planes in the forward direction with some ripples and a significant radiation in the backward direction. The pattern is not rotationally symmetric for E and H planes and seems to be much thinner in the H plane. The measurements of Figure 6(b) show a quasi identical omnidirectional radiation patterns in both E and H planes. The measured gains at 39 GHz are respectively $\sim 4.7\,\text{dB}$ and $\sim 4\,\text{dB}$.

4. HIGH IMPEDANCE SURFACES BASED ANTENNAS

Figure 7(a) shows the proposed HIS based patch antenna. The conventional patch antenna element is surrounded by the mushroom-like HIS. Figures 6(b) and 6(c) show the two realized antenna prototypes surrounded respectively by 2 and 3 layers of unit cells HIS. The Duroid substrate dielectric is relatively thick for the operational frequency and may give rise to the surface wave generation [6–9].
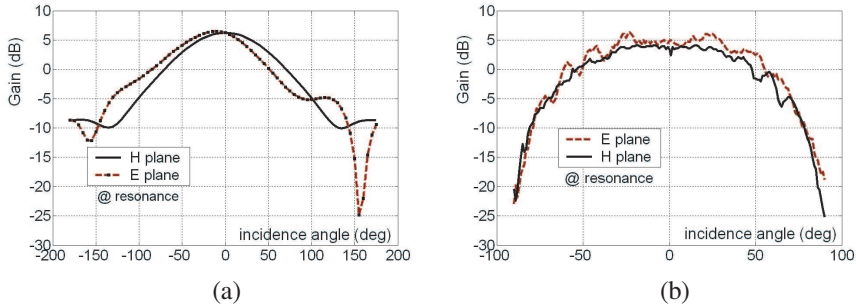
(a)   (b)

Figure 6. Calculated and measured radiation patterns of the patch antenna on the E and H planes.

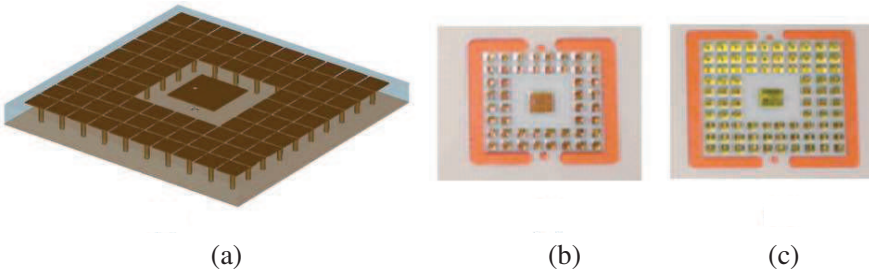(a)   (b)   (c)

Figure 7. (a) HIS surrounding a coax fed patch antenna, (b) and (c) the realized antenna prototypes embedded respectively in 2 layers of HIS (b) and in 3 layers of HIS (c).

The distance between the antenna radiating element and HIS layers is optimized to achieve the best antenna return loss with identical patch elements. In this configuration, the exiting surface waves which diffract and radiate from the edges of the finite substrate are suppressed by the HIS [6–9, 10, 11]. This decreases the ripples and the backward in the antenna radiation patterns.

Figures 8(a) and 8(b) show the calculated and measured return losses (S_{11}) of the HIS based antenna prototypes and in comparison, those of the conventional antenna. When the antenna is surrounded by the HIS layers, it offers higher bandwidth. Compared to the measurements, the simulations show that the resonance frequency shifts slightly to higher frequencies. The measurement results show a unique 39.5 GHz resonance frequency for the three prototypes. A better antenna matching is obtained with the 3 HIS layers.
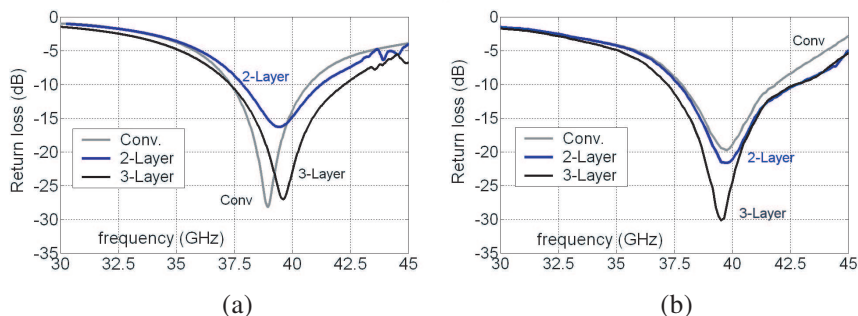
Figure 8. Comparison of the FDTD calculated (a) and the measured (b) antenna return loss (S_{11}) of the prototype antennas.

The measured bandwidth is of $\sim 12\%$ from 38 to 42 GHz for the conventional patch antenna, of $\sim 13\%$ from 37.5 to 43 GHz for the 2 HIS layers and of $\sim 15\%$ from 37.2 to 43 GHz for the last 3-layer HIS prototype antenna.

To understand the role of the HIS, we come back to Figure 4 which shows the sensitivity of the bandgap with the number of elementary cell layers surrounding the antenna. For each additional layer, the band gap expands and its attenuation becomes more important. The reflection coefficients of HIS based antennas using 4-Layer and 5-Layer are simulated for the same patch element. In comparison to the 3-Layer case, there is no significant difference in the bandwidth (below -10 dB) and on the resonance frequency. Moreover, the 4-Layer S_{11} response is the same as that obtained for the 3-Layer. A better adaptation is observed for the 5-Layer case. The criterion seems to be rather the achieved attenuation within the band gap of the N unit cell HIS. The 2-layer structure achieves a theoretical attenuation of -20 dB around 40 GHz, and this is insufficient to improve the matching of the antenna but helps to increase its bandwidth to $\sim 13\%$. The 3-layer structure makes a theoretical attenuation of -30 dB over a wide band around 40 GHz. The surface currents are efficiently attenuated. This contributes to improve the adaptation and the antenna bandwidth to $\sim 15\%$.

The antenna radiation patterns are measured at the resonance frequency for the three prototypes in E and H planes (Figure 9). The level at boresight is slightly higher for the 3-Layer HIS. Since the radiation patterns are measured only from -90 to 90 deg, the backward radiation patterns are not shown in the Figure 9. To show the surface wave suppression effect, we have calculated the near field around the patch antenna for the 3-layer HIS design. Figure 10 shows the electric
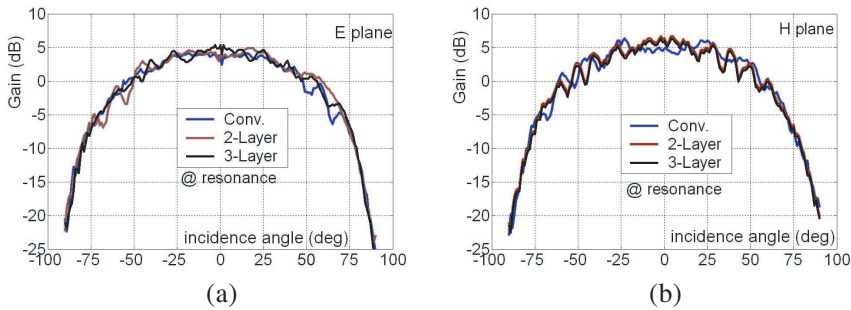
(a)   (b)

Figure 9. The measured radiation patterns of antenna prototypes; the E-plane (a) and the H-plane (b).

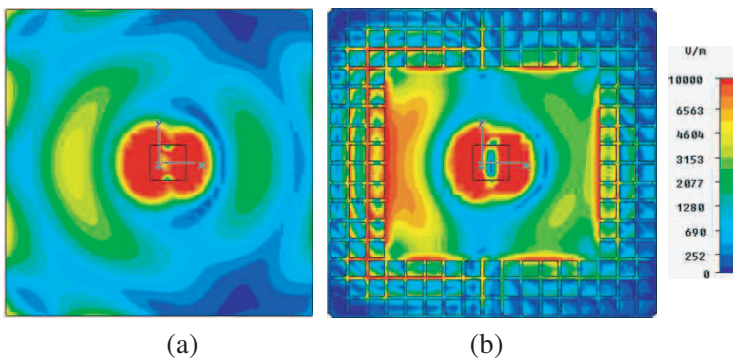(a)   (b)

Figure 10. Near field distribution at 39 GHz, (a) the conventional patch antenna and (b) the 3-Layer HIS patch antenna.

field distribution. For the HIS based antenna, the induced currents are restricted to a localized region around the patch antenna. They never reach the edges of the finite substrate. The surface wave suppression gives a higher radiation level at boresight (Figure 9).

Figure 11 depicts the radiation patterns of the 3-Layer antennas measured in the E plane for the principal (co) polarization in the frequency range of 38–45 GHz. The results demonstrate a large bandwidth around 15% between 38 and 44 GHz with a gain of ~ 5 dB.

The cross-polar patterns of the antennas are plotted in Figure 12 at their respective resonance frequency. The cross-polarization levels are lower on the radiation patterns of the HIS based antennas. The measured data show that the cross-polarized wave is suppressed by using the HIS. In particular, the cross-polarization levels at the ± 90 deg direction are 7 dB lower than in the conventional antenna configuration.
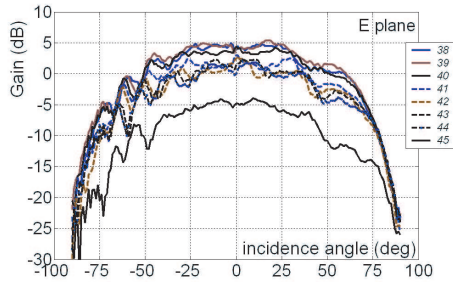
Figure 11. Antennas bandwidth, measured radiation patterns of the metamaterial antenna 3-Layer prototype.
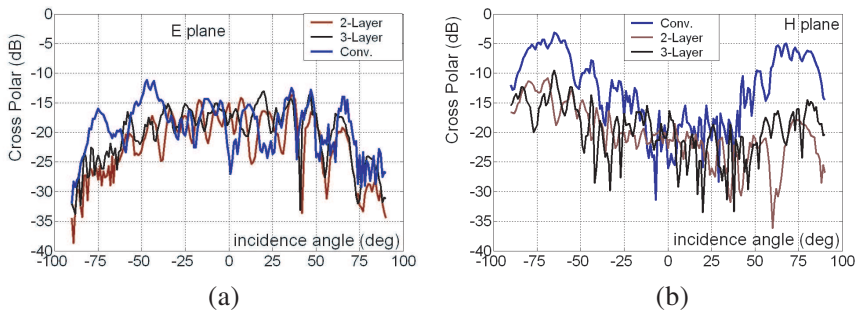

Figure 12. The measured Cross Polar radiation patterns, comparison between the conventional patch antenna and the metamaterial antenna; (a) in the H plane and (b) in the E plane.

5. CONCLUSION

40 GHz-Antenna prototypes have been investigated for high data rate communications. Millimeter wave High Impedance Surfaces (HIS) with finite area sizes are used to control the near field distributions. The return loss and radiation patterns have been analyzed for each prototype using numerical simulations and measurements. The obtained results demonstrate the effect of the HIS on the antenna performances. With the 3-layer HIS based antenna, a large bandwidth of $\approx 15\%$ is achieved around 40 GHz with a high gain of $\sim$5–6 dB and a significant reduction of the cross polarization radiation patterns.

REFERENCES

1. Costanzo, S., I. Venneri, G. Di Massa, and G. Amendola, "Hybrid array antenna for broadband millimeter-wave applications," *Progress In Electromagnetics Research*, PIER 83, 173–183, 2008.

2. Cui, B., J. Zhang, and X. W. Sun, "Single layer micro-strip antenna arrays applied in millimeter-wave radar," *Journal of Electromagnetic Waves and Applications*, Vol. 22, No. 1, 3–15, 2008.

3. Ren, Y.-J. and K. Chang, "An ultrawideband microstrip dual ring antenna for millimeter-wave applications," *IEEE Antennas and Wireless Propagat. Letters*, Vol. 6, 457–459, 2007.

4. Yang, G.-M., R. Jin, J. Geng, and W. He, "Planar broadband millimeter-wave antenna based on open loop ring resonators," *Microwave and Optical Technology Letters*, Vol. 50, No. 2, 324–328, 2008.

5. Navarro, J., "Wide-band, low-profile millimeter-wave antenna array," *Microwave and Optical Technology Letters*, Vol. 34, No. 4, 253–255, 2002.

6. Jackson, D. R., J. T. Williams, A. K. Bhattacharyya, R. L. Smith, S. J. Buchheit, and S. A. Long, "Microstrip patch designs that do not excite surface waves," *IEEE Transactions on Antennas and Propagation*, Vol. 41, No. 8, 1026–1037, August 1993.

7. Mahmoud, S. F. and A. R. Al-Ajmi, "A novel microstrip patch antenna with reduced surface wave excitation," *Progress In Electromagnetics Research*, PIER 86, 71–86, 2008.

8. Sievenpiper, D., "High impedance electromagnetic surfaces," Ph.D. Thesis, UCLA, 1999.

9. Sievenpiper, D., L. Zhang, R. F. J. Broas, N. G. Alexópoulos, and E. Yablonovitch, "Artificial Magnetic conductor Surfaces with a forbidden frequency band," *IEEE Trans. Microw. Theory Tech.*, Vol. 47, No. 11, 2059–2074, 1999.

10. Liang, L., C. H. Liang, L. Chen, and X. Chen, "A novel broadband EBG using cascaded mushroom-like structure," *Microwave and Optical Technology Letters*, Vol. 50, No. 8, 2170–2167, 2008.

11. Mahdi Moghadasi, S., A. R. Attari, and M. M. Mirsalehi, "Compact and wideband 1-D mushroom-like EBG filters," *Progress In Electromagnetics Research*, PIER 83, 323–333, 2008.

12. Bahrami, H., M. Hakkak, and A. Pirhadi, "Analysis and design of highly compact bandpass waveguide filter using complementary split ring resonators (CSRR)," *Progress In Electromagnetics Research*, PIER 80, 107–122, 2008.

13. Yang, F. and Y. Rahmat-Samii, "Microstrip antennas integrated with electromagnetic band-gap (EBG) structures: A low mutual coupling design for array applications," *IEEE Transactions on Antennas and Propagation*, Vol. 51, No. 10, 2936–2946, Oct. 2003.

14. Maslovski, S., P. Ikonen, C. Simovski, M. Karkkainen, S. Tretyakov, and V. Denchev, "Improving antenna near-field pattern by use of artificial impedance screens," physics/0504123, 2005.

15. Wu, Z.-H. and W. X. Zhang, "On profile thickness of printed compound air-fed array antenna," *Journal of Electromagnetic Waves and Applications*, Vol. 24, 199–207, 2010.

16. Sohn, J. R., K. Y. Kim, H.-S. Tae, and J. -H. Lee, "Comparative study on various artificial magnetic conductors for low-profile antenna," *Progress In Electromagnetics Research*, PIER 61, 27–37, 2006

17. Yang, F. and Y. Rahmat-Samii, "Reflection phase characterizations of the EBG ground plane for low profile wire antenna applications," *IEEE Transactions on Antennas and Propagation*, Vol. 51, No. 10, 2939–2949, 2003.

18. Tretyakov, S. A. and C. R. Simovski, "Wire antennas near artificial impedance surfaces," *Microwave and Optical Technology Letters*, Vol. 27, No. 1, 46–50, 2000.